Rapid water transport by long-lasting modon eddy pairs in the southern midlatitude oceans

Chris W. Hughes[1]**, Peter I. Miller**[2]

[1]School of Environmental Sciences, University of Liverpool and National Oceanography Centre, Liverpool, UK
[2]Plymouth Marine Laboratory, Plymouth, UK

Key Points:

- Nine examples of long-lived modon eddy-pairs are identified in the ocean using satellite altimetry.
- The modons are capable of carrying water properties at exceptional speeds and unusual directions.
- The evolution of the modons is in line with a range of theoretical predictions.

Corresponding author: Chris Hughes, `cwh@liv.ac.uk`

Abstract

Water in the ocean is generally carried with the mean flow, mixed by eddies, or transported westward by coherent eddies at speeds close to the long baroclinic Rossby wave speed. Modons (dipole eddy pairs) are a theoretically predicted exception to this behaviour, which can carry water to the east or west at speeds much larger than the Rossby wave speed, leading to unusual transports of heat, nutrients and carbon. We provide the first observational evidence of such rapidly moving modons propagating over large distances. These modons are found in the midlatitude oceans around Australia, with one also seen in the South Atlantic west of the Agulhas region. They can travel at more than ten times the Rossby wave speed of 1–2 cm s^{-1}, and typically persist for about six months carrying their unusual water mass properties with them, before splitting into individual vortices which can persist for many months longer.

1 Introduction

A recent census of mesoscale sea level anomaly propagation [*Chelton et al.*, 2011] has shown that, be they wave-like or eddy-like, almost all anomalies propagate to the west at close to the long baroclinic Rossby wave speed. Where they propagate to the east, they are in eastward-flowing currents which are faster than the Rossby wave speed, and are in fact still propagating to the west relative to the flow. The census showed that the vast majority are eddy-like, in the sense that the ratio U/c of circulatory flow speed U to propagation speed c is significantly larger than 1, a qualitative measure suggesting that water is carried along with the eddy for a short time at least. The Rossby wave speed itself is highly dependent on latitude, being faster than 10 cm s^{-1} over parts of the tropics, but below about 5 cm s^{-1} outside the tropics, decreasing to below 1 cm s^{-1} at latitudes beyond about 40–45° north or south.

It may seem surprising that nonlinear eddies propagate at the linear Rossby wave speed, but this is in line with theoretical predictions. *McWilliams and Flierl* [1979] showed that (for a single vertical mode) the centre of mass of any quasigeostrophic disturbance moves at the long Rossby wave speed. The centre of mass may not be the vortex centre if it radiates Rossby waves, but the Rossby wave radiation is generally a weak perturbation which slightly slows propagation and causes cyclonic vortices to drift poleward, and anticyclonic vortices to drift equatorward [*Flierl*, 1984; *McDonald*, 1998; *Nycander*, 2001]. A strong association of meridional motion with sense of eddy rotation was found in the south Indian Ocean near to Australia [*Morrow et al.*, 2004]. A weaker, but statistically clear association was also supported by *Chelton et al.* [2011]; although only a weak bias was observed for cyclonic eddies, 70% of long-lived anticyclonic eddies drifted equatorward.

The quasigeostrophic assumption allows for strong nonlinearity in the sense of large U/c, as observed in the ocean. However, it assumes that perturbations will be small in both layer thickness ($\delta H/H \ll 1$ where H is layer thickness and δH is its perturbation) and vorticity ($|\zeta/f| \ll 1$), where ζ is relative vorticity and f is the Coriolis parameter). These latter forms of nonlinearity do perturb the eddy propagation speed, but it still tends to remain close to the Rossby wave speed. The effect of a finite height perturbation is to slow cyclones by at most a factor of two, and to speed up anticyclones to at most the average of Rossby wave speeds at the centre of the eddy and outside it [*Cushman-Roisin et al.*, 1990]. The observed degree of nonlinearity by this measure is much weaker than in U/c, with typical values of $\delta H/H$ being around 0.1 to 0.3 [*Chelton et al.*, 2011].

The third form of nonlinearity comes from breaking the link between layer thickness gradient and flow speed. The relevant parameter, derived by considering cyclostrophic balance in an almost circular eddy, is the Rossby number U/fr where r is the eddy radius, or equivalently $|\zeta/f|$. Although *Chelton et al.* [2011] do not calculate this parameter explicitly, they show that the parameter $U/\beta r^2$ is typically of order 1. Since this is $f/\delta f$

times U/rf, where δf is the change in f over one eddy radius, we can infer that U/rf is generally small. This third form of nonlinearity was dealt with by *Nof* [1981, 1983], who found for an almost circular eddy that this also has the effect of accelerating anticyclones and decelerating cyclones relative to the Rossby wave speed of the surrounding stratification. In the extreme case of a lens of water (layer thickness, and hence Rossby wave speed, is zero outside the lens), *Killworth* [1983] showed that the propagation speed is at most 2/3 of the Rossby wave speed based on the stratification at the centre of the lens, and *Flierl* [1984] showed that it is typically within 40% of the Rossby wave speed based on the average thickness of the lens.

In summary, it seems to be a very robust result that monopolar vortices drift predominantly westwards at a speed close to the long baroclinic Rossby wave speed. The reason for the robustness of this result is given by *Nycander* [1996], who notes that it is essentially conservation of angular momentum, in a manner analogous to the precession (slow rotation of the axis) of a gyroscope. This robustness means that the bulk motion of water must generally be carried along with the mean flow, or with eddies moving at or close to the Rossby wave speed, except where they interact with topography.

There is, however, an exception to this. The constraint is on the motion of the centre of mass of the eddy, but if the eddy has zero net mass anomaly then there is no longer a constraint on the propagation speed. This can be the case for dipolar eddies, with both positive and negative mass and vorticity anomalies coupled together. The archetype of these on a rotating sphere is known as a modon [*Stern*, 1975], and can propagate either to the east or to the west at speeds outside the Rossby wave speed range.

A modon consists of a patch of positive (anticlockwise) relative vorticity to the left of the propagation direction, and a neighbouring patch of negative (clockwise) relative vorticity to the right. The circulation induced by the positive vorticity pushes the negative vorticity forwards, and the circulation induced by the negative vorticity pushes the positive vorticity forwards, so the pair propagate together. The three dimensional analogue of this is the smoke ring or vortex ring of which many long-lived examples are known.

On a sphere or beta plane, steady propagation is only possible in a zonal direction because any northward component of the propagation moves the modon to a region of more positive planetary vorticity. Since it is the sum of planetary and relative vorticity that is conserved (assuming layer thickness anomaly remains constant, because of mass conservation), a northward propagation will weaken the anticlockwise vortex and strengthen the clockise vortex, causing the modon to steer toward the clockwise vortex (i.e. to turn right). If the modon is propagating mainly to the east, this tends to bring it back to its initial latitude and it can continue propagating to the east while oscillating to north and south of the latitude at which the vortices are balanced [*Nycander and Isichenko*, 1990], whereas a westward-propagating modon is unstable and any perturbation will cause it to turn round to the east [*Nycander and Isichenko*, 1990; *Nycander*, 1992; *Hesthaven et al.*, 1993].

Dipolar vortices appear to be common in the ocean, particularly near to eastern boundaries [e.g. *Ikeda et al.*, 1984; *Ahlnäs et al.*, 1987; *Simpson and Lynn*, 1990; *Strub and James*, 2000; *Callendar et al.*, 2011], and in association with western boundary currents [*Hooker et al.*, 1995]. There is also evidence of intermittent pairing of subsurface Meddies in the Gulf of Cadiz [*Hégaret et al.*, 2014], but there appears to be little evidence of stable modons propagating over long distances at a speed outside the Rossby wave range. Our purpose here is to present evidence of a number of such modons in the midlatitude ocean to the north of the Antarctic Circumpolar Current (ACC).

2 Observations

The identification of modons is based on satellite altimeter data, in particular the Segment-Sol multi-missions d'ALTimétrie, Orbitographie et localisation précise/Data Unification and Altimeter Combination System (SSALTO/DUACS) 1/4° gridded absolute dynamic topography using all available satellites, distributed by Aviso. We calculated geostrophic currents based on first order differencing, and made movies of the resulting flow speed. We initially identify candidate modons by visual analysis. Typically, the modons have small length scales and fast speeds, meaning they are poorly resolved in the altimetry in both space and time. They stand out in the movie because of their unusual propagation speed and/or direction, and paired nature. The first modon identified (described as modon E below) stood out very clearly. Having spotted this unusual feature, a global search was undertaken to identify similar events.

The nine modons we have identified are probably the clearest. There is no sharp cut off to what could be considered a modon, and there are many other temporary associations of pairs of vortices, particularly to the southwest and south of Australia, and in the region of formation of Agulhas ring eddies. There are hints of a complex eddy regime in the Pacific off the southern tip of South America, but the relatively small amplitudes and length scales here make interpretation ambiguous. There may also be brief pairings in the Gulf of Alaska, and eddies shed from the southern tip of Madagascar certainly interact [*de Ruijter et al.*, 2004, 2005], but clear evidence of modons is not seen. Movies showing modon propagation are given in the Supporting Information to this paper.

Once a modon has been identified, the best estimate of the centre of each of the component vortices is made by eye for each frame of the movie. This is not always obvious as the modon may appear very stretched out as a result of its speed of propagation, or may be temporarily missed by the satellite measurements, so the individual position estimates should be interpreted with some caution, though the longer-term displacements are clear. Each constituent vortex was tracked both forward and backward in time from a point at which the modon was particularly clear, the tracking being continued for as long as the vortex could be followed. Zonal and meridional propagation velocities were calculated based on 5-day position differences, and a 5-day smoothing was applied to the positions. The positions are tabulated in the Supporting Information. Speeds were calculated from the daily velocity component estimates, and a 15-day smoothing was applied to the speed values.

Figures (1) and (2) summarize the resulting modon tracks. The vorticity maps show geostrophic vorticity ζ divided by f at each grid point, from the time at which that grid point was closest to a vortex centre. These show that the left-hand vortex is anticyclonic (and therefore positive vorticity in the southern hemisphere), and the right-hand vortex is cyclonic as expected. They also show that the Rossby number $|\zeta/f|$ is typically around 0.1–0.3, though at times it appears to intermittently weaken as expected when small scales are missed in the mapping of altimeter data. Away from the modon tracks, the vorticity is effectively from a random time, and shows the typical amplitudes to be expected.

On the propagation speed plots, unfilled black circles indicate every 30th day, and the black spot indicates the date marked on the panel, which was the start date for eddy tracking. Smaller circles are later in time to make the propagation direction clear. In many cases, the modon speed is of order 10–20 cm s^{-1}. In comparison, the linear long baroclinic Rossby wave speeds in these regions [*Chelton et al.*, 1998] vary from 1.2 cm s^{-1} (modons A–E) to 2.2 cm s^{-1} (modon H), so the modon speeds can be more than ten times the Rossby wave speed.

Often, one or both of the constituent vortices can be followed for some considerable time after the modon splits apart. In these cases, the propagation speed for the monopolar vortices is substantially slower than for the modon but, interestingly, often still faster
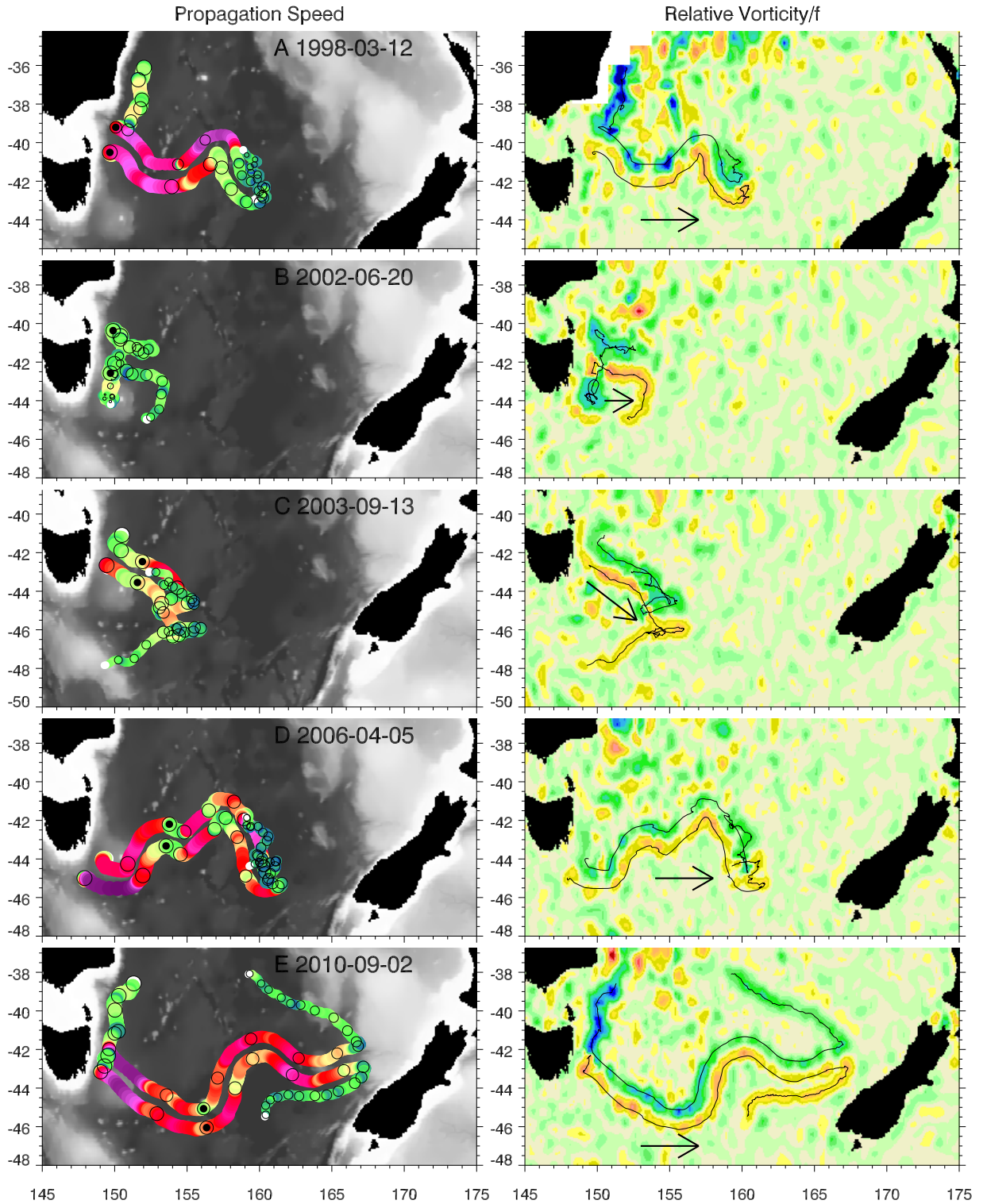
Figure 1. Summary of Tasman Sea modon trajectories, showing (left) their speed (the grey background shows bathymetry) and (right) associated relative vorticity. The dates given are at the time of the filled black dot, with open circles every 30 days. Arrows indicate the propagation direction. See Figure (2) for the scales.
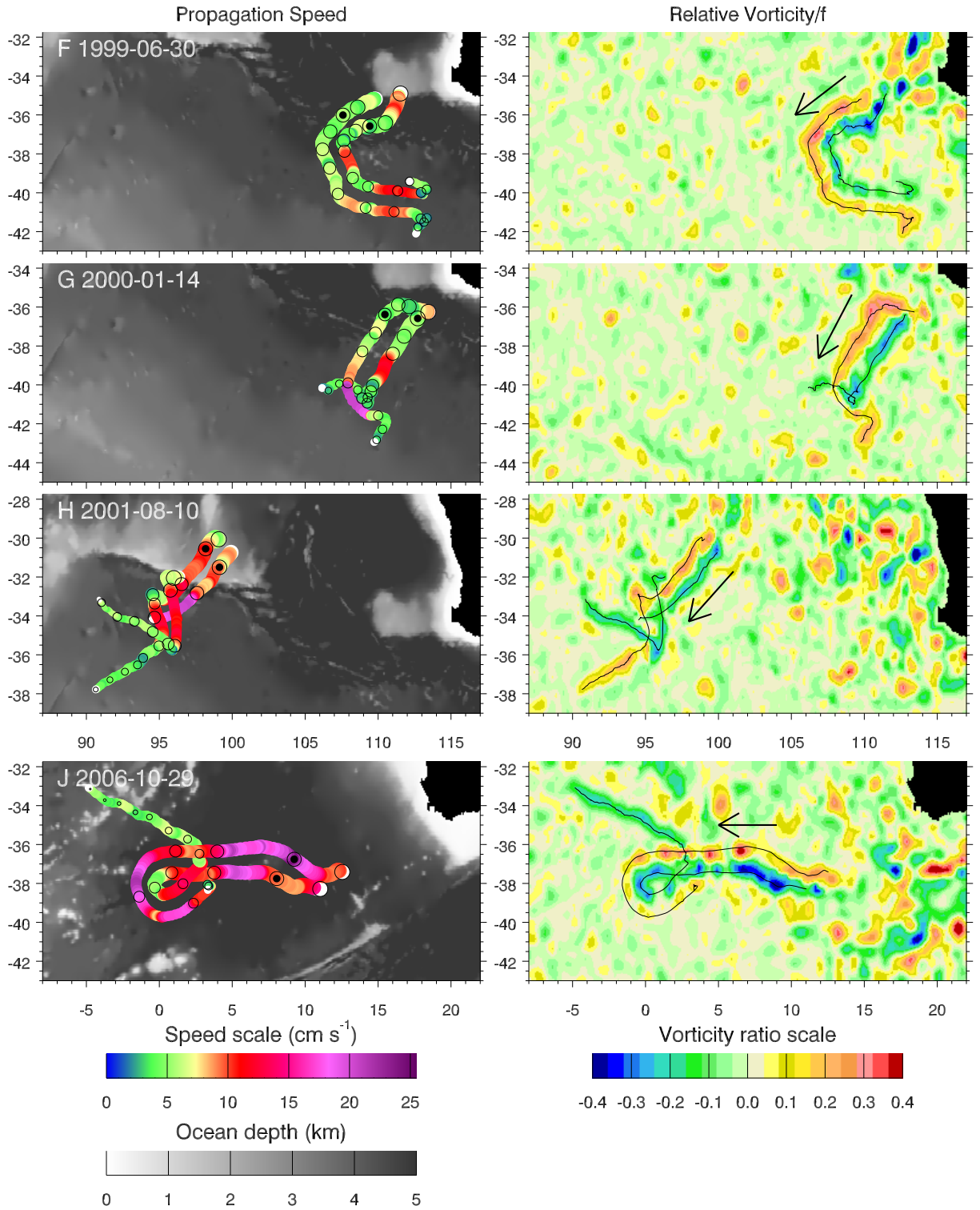
Figure 2.   Summary of initially westward modon trajectories, as in Figure (1).

than the Rossby wave speed, even though the separated eddies are in regions of weak eastward flow. Counterintuitively, a surface-intensified eastward mean flow can increase the westward long Rossby wave speed by up to a factor of 2 [*Colin de Verdière and Tailleux*, 2005], but this does not appear sufficient to explain the observed speeds. Almost always, the anticyclonic vortex propagates equatorward and west, and the cyclonic vortex propagates poleward and west, as predicted by theory. Exceptions are the anticyclonic vortex from modon B, which reaches the continental slope and then propagates poleward, and the cyclonic vortex of modon D, which wanders slowly equatorward.

The eastward-propagating modons A–E all continue to propagate to the east, though they may meander, until they split. Modon C is interesting in that it propagates to the southeast, then appears to split and the individual vortices (particularly the northern one) drift slowly west before joining together again and propagating once more to the east, before finally splitting and separating. These modons all form from eddies on the Australian continental slope, which generally propagate slowly to the south along the slope until they pair into a modon somewhere in the vicinity of Tasmania. Modon E is the clearest of all examples, with one precursor eddy visible well before formation of the modon, and both constituent vortices remaining coherent for almost a year after splitting.

Modons F-H all form to the west or southwest of Australia, in the open ocean region which has already been noted for the different propagation of cyclonic and anticyclonic monopolar eddies [*Morrow et al.*, 2004]. The modons form in the open ocean and propagate initially to the southwest. Modons F and G turn to the east before splitting, whereas modon H starts as a pair, but the left-hand vortex is lost and the right-hand vortex pairs up with a new partner and propagates to the south before splitting. These modons tend not to maintain speeds as fast as observed in the eastward-propagating pairs, but are still substantially faster than baroclinic Rossby waves.

Finally, modon J forms to the southwest of South Africa, close to the Agulhas eddy formation region. It propagates rapidly almost due west before suddenly turning back to the east and splitting. The left-hand vortex can then be tracked for a further 8 months. It should be noted that there is no clear sign of the right-hand vortex during the period of rapid reversal, though it reappears shortly before the modon splits.

There is no clear trigger for the modons to split in most cases. Modon E stalls and splits after reaching the New Zealand continental slope, and seamounts may be responsible for the splitting of modon B and the double end-point of modon C, but there is no obvious topographic influence in other cases.

All of the vortices identified here are present in some form in the *Chelton et al.* [2011] eddy database, though often in partial or disjointed ways. For example, the western half of the track of the left-hand vortex of modon E is represented as two separate eddies, the right-hand vortex of E is only represented before it leaves the continental slope, and only a very short section of the left-hand vortex of D is present. In contrast, modons B, F and G, and the left-hand vortex of J, are very similar in the eddy database. Overall, understandably, the *Chelton et al.* [2011] method is more successful at tracking the more slowly propagating sections of vortex paths.

3 Temperature and modon E

The previously cited observations of dipole eddies all focus on sea surface temperature measurements. This has the advantage of higher spatial resolution, but the disadvantage of intermittently being obscured by cloud cover. It is interesting therefore to see how these modons, identified in satellite altimetry, influence sea surface temperature. We illustrate this in figure (3), for the case of the clearest modon: modon E. Temperatures here are taken from the NASA Multi-Sensor Merged Ultra-High Resolution (MUR) SST dataset, acquired via OpenDAP in geographic projection at daily 1km resolution. In order

to enhance the eddy structures for animation (Supporting Information), thermal composite front maps [*Miller*, 2009] were generated from the MUR daily data over rolling 3-day periods, using a minimum SST step across the front of 0.4 °C.

Figure (3) clearly shows temperature signals throughout the life of the modon. The chosen times are from days with good cloud-free coverage over the modon, giving higher spatial resolution than at times which rely on microwave temperature measurements. The temperature anomalies can generally be interpreted as a combination of advection by the vortices and stirring of the background temperature field, and show coherent advection with the vortex cores. Temperature is sometimes homogenized in each vortex, but on occasions (e.g. December 2010) there is clear evidence of winding of an entrained temperature anomaly within a vortex.

The temperature signals after the modon has split into two isolated eddies become more subtle, but are still visible for many months. These surface waters are subject to rapid heat exchange with the atmosphere, and also to surface Ekman currents which need not follow the quasigeostrophic flow, so that surface temperature is not an advectively conserved quantity.

These panels are repeated at larger scale in Supplementary Figure 1, together with equivalent scenes from all the other modons which overlap the temperature dataset in time (B–D and J), showing that the temperature signal is not limited to modon E. In particular, the temperature snapshots confirm the presence of the right-hand vortex in modon J during the time when it reverses direction and becomes impossible to distinguish in the altimeter data.

In the case of Modon E, there are enough times at which the modon is visible in the temperatures that it is possible to refine the modon trajectory. This is done, as before, by eye, using the positions derived from altimetry as a guide. With the refined trajectory we can then define a moving coordinate system which is centered on the modon, and oriented along its 5-day mean propagation direction. Assuming the modon spatial structure is constant to first order, this then allows us to use along-track satellite altimeter measurements (Jason-1, Jason-2 and Envisat data are available over this period, also provided by CMEMS) to map the modon without the blurring effect of the gridding process. The resulting mean modon structure is shown in Figure (3b), after Gaussian smoothing with a radius at half-maximum of 20 km (Supplementary Figure 2 shows how the smoothing affects the structure).

This shows how the modon appears in the dynamic topography. In order to see whether fluid moves with the modon, we need to see the flow relative to the modon. We show this in Figure (3c), in which we add a north-south slope equivalent to a geostrophic westward speed of 8.8 cm s^{-1}, the mean speed of the modon over the averaging period. This clearly shows a region of recirculating flow, moving with the modon, out to a radius of about 100 km. In fact, such recirculations remain clear if we assume propagation speeds of up to 50 cm s^{-1}, albeit with a reduced trapping radius. The non-steady nature of the true vortices means that the outer parts of the vortices are likely to intermittently exchange fluid with the surroundings.

In Figure (3d), we show the best-fitting analytical modon solution taken from the solution of *Larichev and Reznik* [1976] as described in more detail by *Flierl et al.* [1980]. This solution requires as input parameters the latitude, 44°S; baroclinic Rossby radius, 27 km from *Chelton et al.* [1998]; propagation speed (8.8 cm s^{-1}); and trapping radius, chosen as 100 km, which gives the best fit to the observations. The amplitude of the modon is determined as part of the solution, so the simultaneous matching of the analytical modon radius and amplitude to the observations is further evidence that the observed feature is indeed a modon.
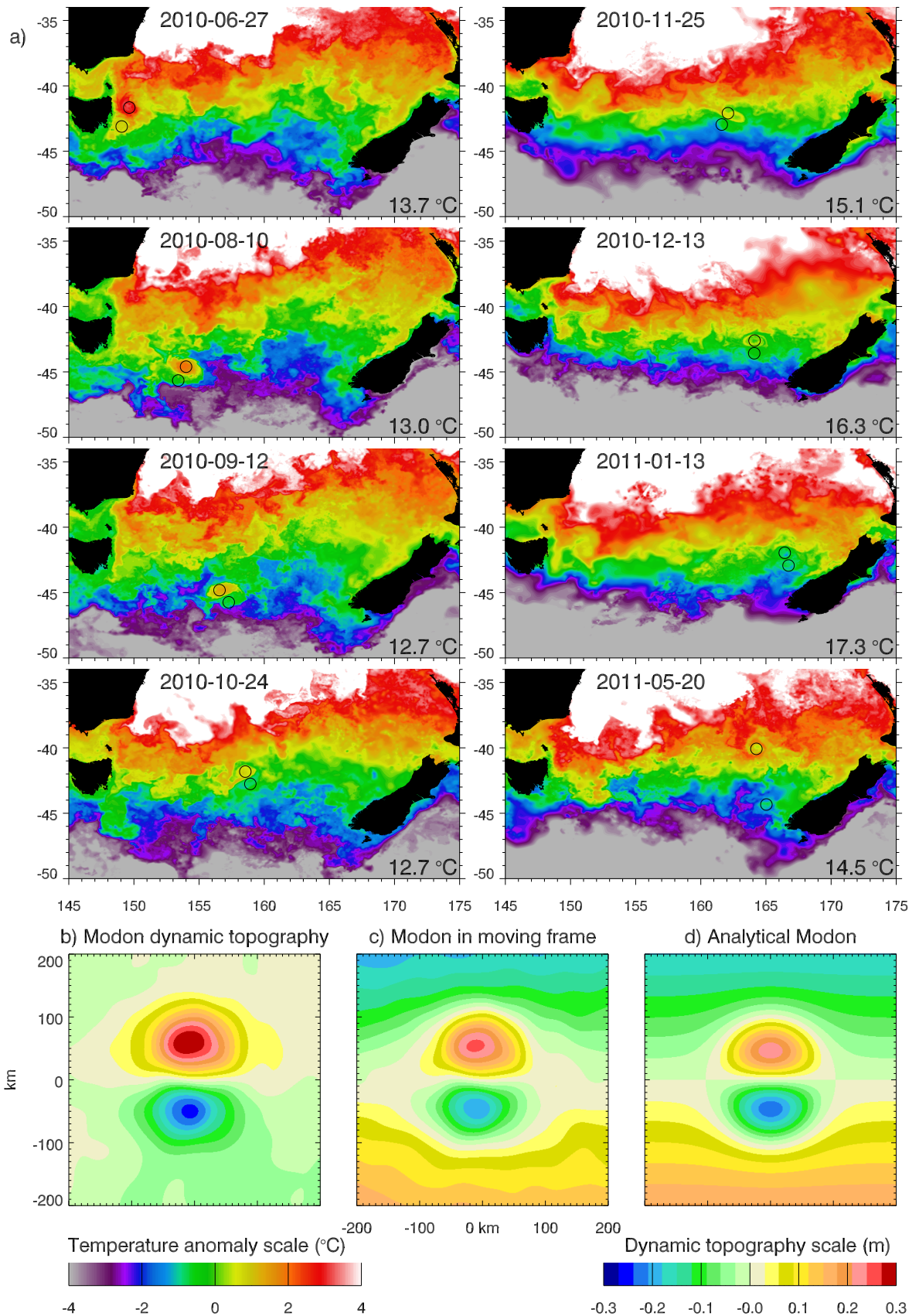
Figure 3. a) Sea surface temperature associated with modon E. Black circles mark the modon position as determined from sea level. Temperatures are shown relative to the median value, which is written on each plot. Colors saturate at ±4 °C. b) The mean sea level structure of modon E from along-track altimetry. c) as in b) but with a north-south slope added so that contours represent the flow relative to the modon. d) the analytical modon solution which best fits the observations

4 Summary and discussion

We have shown that modons can be found intermittently in the southern midlatitude region north of the ACC. Of the nine modons identified between 1993 and May 2016, five are formed on the continental slope east of Tasmania, and propagate eastward across part or all of the Tasman Sea. The other modons form in the open ocean, in regions rich with eddies, and propagate initially to the west or southwest. This suggests two different formation mechanisms.

An isolated ocean feature must have zero net relative vorticity (otherwise it induces a circulation out to all distances and cannot be considered isolated). A monopolar eddy consists of a core with relative vorticity of one sign, surrounded by a ring of opposite-signed relative vorticity. In contrast, a modon is two neighbouring patches of opposite-signed relative vorticity. Two possible mechanisms for formation of modons are for a pair of opposite-signed monopolar vortices to approach each other and for their outer rings of vorticity to be stripped off as they link together, or for the outer ring of a single vortex to be stripped off and form into a neighbouring patch, converting the monopole to a dipole. *Southwick et al.* [2015] illustrate how a monopolar vortex, propagating parallel to a coastline, and approaching a corner, can induce a complementary vortex at the corner and then propagate away from the coast as a dipole (the dynamics are f-plane). Alternatively, *Callendar et al.* [2011] find a case in which tidal currents repeatedly generate separate regions of positive and negative relative vorticity near to Cape St. James on the southern tip of the Canadian Pacific island of Haida Gwaii (Queen Charlotte Islands). The repeated forcing builds up a pair of complementary vortices which then join together and propagate away to the southwest. In a third mechanism, *Manucharyan and Timmermans* [2013] model examples of eddy pairs generated at an unstable front, in an f-plane Arctic context, and *Brannigan et al.* [2017] show how differing vertical structures of the component eddies can influence the propagation. Here, we have only surface information, so cannot say anything about the vertical structure beyond what is implied by the effectiveness of the first baroclinic mode analytical modon solution in explaining the observations.

From our data it is difficult to determine the formation mechanism. Precursor eddies are rarely distinguishable, though for the Tasman Sea modons the anticyclonic vortex can sometimes be seen propagating down the Australian coast for some time before pairing up with an opposite vortex in the vicinity of Tasmania, which is reminiscent of the *Southwick et al.* [2015] mechanism, though it should be noted that there is significant variation in the position at which pairing occurs. It is quite striking in the animations how rapid the initial propagation can be after pairing, giving the appearance of a jet squirting out from the coast before settling into a modon form. For the open ocean cases it is even less common to see precursor eddies, but the many monopolar eddies in these regions suggest that a chance pairing of two complementary vortices is likely in these regions. If anything, it is surprising that we only have one example in the Atlantic sector, given how energetic the Agulhas region is.

Aside from their interest as confirmation of a theoretically predicted mode, these modons may play an important wider role in the ocean. Especially in the Tasman Sea, they represent an unusual pathway for propagation of water with different properties into the open ocean. *Baird and Ridgway* [2012] have shown that anticyclones propagating to the south along the Australian continental slope contain a deep oxygen and salinity maximum which is identified as Bass Strait Water from the shelf between Tasmania and mainland Australia. They suggest that this unusual water mass may have important ecological consequences, reducing nutrient availability in the euphotic zone and encouraging deep water pelagic fish populations. The fact that some of these eddies shoot rapidly across the Tasman Sea introduces a new pathway and range of influence for these Bass Strait Waters, as well as other water masses associated with the eddies.

It is worth noting again that, despite the many successes of theoretical predictions in accounting for this observed behaviour, the typical westward propagation speeds of monopolar eddies following the splitting of the modons is clearly faster than the linear baroclinic Rossby wave speed. As this is the case for both cyclonic and anticyclonic eddies, it cannot be due to any of the nonlinear effects discussed above. Since the general theoretical results tend to rely on the presence of only one active vertical mode, this might be evidence that the baroclinic mode alone is insufficient to describe the eddy behaviour.

Finally, it is worth emphasizing that the rapid propagation speed and small size of these modons puts them at the limit of spatial and temporal resolution of the present satellite altimeter system. We can expect significantly better sampling from swath altimetry such as the Surface Water Ocean Topography mission [*Fu and Ferrari*, 2008], which will permit these phenomena to be resolved more clearly, and perhaps to be seen in other regions of the ocean. As a comparison, given a 21-day repeat orbit and swath width of 120 km for SWOT, we would expect at the latitude of modon E to obtain a complete map (measurements within 5 km of each point) on average every 7.5 days. For the 3-satellite sampling of modon-E, every 7.5 days we have on average a single satellite pass within 23 km of a vortex centre. To get within 5 km we have to wait an average of 59 days. The resulting better resolution from SWOT may make it possible to identify modons automatically and to quantify their coherent transport, using Lagrangian techniques such as the coherent vortex identification method of *Haller and Beron-Vera* [2013].

References

Ahlnäs, K., T. C. Royer, and T. H. George (1987), Multiple dipole eddies in the Alaska Coastal Current detected with Landsat thematic mapper data, *J. Geophys. Res.*, 92(C12), 13041–13047, doi:10.1029/JC092iC12p13041.

Baird, M. E., and K. R. Ridgway (2012), The southward transport of sub-mesoscale lenses of Bass Strait Water in the centre of anti-cyclonic mesoscale eddies, *Geophys. Res. Lett.*, 39, L02603, doi:10.1029/2011GL050643.

Brannigan, L., H. Johnson, C. Lique, J. Nycander and J. Nilsson (2017), Generation of sub-surface anticyclones at Arctic surface fronts due to a surface stress , *J. Phys. Oceanogr.*, doi:10.1175/JPO-D-17-0022.1, in press.

Callendar, W., J. M. Klymak, and M. G. G. Foreman (2011), Tidal generation of large sub-mesoscale eddy dipoles, *Ocean Sci.*, 7, 487–502, doi:10.5194/os-7-487-2011.

Chelton, D. B., R. A. deSzoeke, M. G. Schlax, K. El Naggar, and N. Siwertz (1998), Geographical variability of the first baroclinic Rossby radius of deformation, *J. Phys. Oceanogr.*, 28, 433–460, doi:10.1175/1520-0485(1998)028<0433:GVOTFB>2.0.CO;2.

Chelton, D. B., M. G. Schlax, and R. M. Samelson (2011), Global observations of nonlinear mesoscale eddies, *Prog. Oceanogr.*, 91, 167–216, doi:10.1016/j.pocean.2011.01.002.

Colin de Verdière, A. and R. Tailleux (2005), The interaction of a baroclinic mean flow with long Rossby waves, *J. Phys. Oceanogr.*, 35, 865–879, doi: 10.1175/JPO2712.1.

Cushman-Roisin, B., E. P. Chassignet, and B. Tang (1990), Westward motion of mesoscale eddies, *J. Phys. Oceanogr.*, 20, 758–768, doi:10.1175/1520-0485(1990)020<0758:WMOME>2.0.CO;2.

de Ruijter, W. P. M., H. M. van Aken, E. J. Beier, J. R. E. Lutjeharms, R. P. Matano, and M. W. Schouten (2004), Eddies and dipoles around South Madagascar: formation, pathways and large-scale impact, *Deep-Sea Res. I*, 51, 383–400, doi:10.1016/j.dsr.2003.10.011.

de Ruijter, W. P. M., H. Ridderinkhof, and M. W. Schouten (2004), Variability of the southwest Indian Ocean, *Phil. Trans. R. Soc. A*,363, 63–76, doi:10.1098/rsta.2004.1478.

Flierl, G. R., (1984), Rossby wave radiation from a strongly nonlinear warm eddy, *J. Phys. Oceanogr.*, 14, 47–58, doi:10.1175/1520-0485(1984)014<0047:RWRFAS>2.0.CO;2.

Flierl, G. R., V. D. Larichev, J. C. McWilliams and G. M. Reznik (1980), The dynamics of baroclinic and barotropic solitary eddies, *Dyn. Atmos. Oceans*, 5, 1–41, doi: 10.1016/0377-0265(80)90009-3

Fu, L.-L., and R. Ferrari (2008), Observing oceanic submesoscale processes from space, *Eos Trans. AGU*, 89(48), 488–488, doi:10.1029/2008EO480003.

Haller, G., and F. J. Beron-Vera (2013), Coherent Lagrangian vortices: the black holes of turbulence, *J. Fluid Mech.*, 731, R4, doi:10.1017/jfm.2013.391.

Hégaret, P. L., X. Carton, I. Ambar, C. Ménesguen, B. L. Hua, L. Chérubin, A. Aguiar, B. Le Cann, N. Naniault, and N. Serra (2014), Evidence of Mediterranean Water dipole collision in the Gulf of Cadiz, *J. Geophys. Res. Oceans*, 119, 5337–5359, doi:10.1002/2014JC009972.

Hesthaven, J, S., J. P. Lynov, and J. Nycander (1993), Dynamics of nonstationary dipole vortices, *Phys. Fluids A*, 5(3), 622–629, doi:10.1063/1.858648.

Hooker, S. B., J. W. Brown, A. D. Kirwan Jr., G. J. Lindemann, and R. P. Mied (1995), Dynamics of a warm-core dipole ring, *J. Geophys. Res. Oceans*, 100(C12), 24,797–24,809, doi:10.1029/95JC02900.

Ikeda, M., L, A. Mysak, and W. J. Emery (1984), Observation and modeling of satellite-sensed meanders and edies off Vancouver Island, *J. Phys. Oceanogr.*, 14, 3–21, doi:10.1175/1520-0485(1984)014<0003:OAMOSS>2.0.CO;2.

Killworth, P. D. (1983), On the motion of isolated lenses in a beta plane, *J. Phys. Oceanogr.*, 13, 368–376, doi:10.1175/1520-0485(1983)013<0368:OTMOIL>2.0.CO;2.

Larichev, V. D. and G. M. Reznik (1976), Two-dimensional solitary Rossby waves, *Doklady Akad. Nauk SSSR*, 231, 12–13.

Manucharyan, G. E. and M. -L. Timmermans (2013), Generation and separation of mesoscale eddies from surface ocean fronts, *J. Phys. Oceanogr*, 43, 2545–2562, doi: 10.1175/JPO-D-13-094.1.

McDonald, N. R. (1998), The decay of cyclonic eddies by Rossby wave radiation, *J. Fluid Mech.*, 361, 237–252, doi:10.1017/S0022112098008696.

McWilliams, J. C., and G. R. Flierl (1979), On the evolution of isolated, nonlinear vortices, *J. Phys. Oceanogr.*, 9, 1155–1182, doi:10.1175/1520-0485(1979)009<1155:OTEOIN>2.0.CO;2.

Miller, P. I. (2009), Composite front maps for improved visibility of dynamic sea-surface features on cloudy SeaWiFS and AVHRR dat, *J. Mar. Sys.*, 78, 327–336, doi:10.1016/j.jmarsys.2008.11.019.

Nof, D. (1981), On the β-induced motion of isolated baroclinic eddies, *J. Phys. Oceanogr.*, 11, 1662–1672, doi:10.1175/1520-0485(1981)011<1662:OTIMOI>2.0.CO;2.

Nof, D. (1983), On the migration of isolated eddoes with application to the Gulf Stream, *J. Mar. Res.*, 41(3), 399–425, doi:10.1357/002224083788519687.

Nycander, J. (1992), Refutation of stability proofs for dipole vortices, *Phys. Fluids A*, 4, 467–476, doi:0.1063/1.858319.

Nycander, J. (1996), Analogy between the drift of planetary vortices and the precession of a spinning body, *Plasma Phys. Rep.*, 22(9), 771–774.

Nycander, J. (2001), Drift velocity of radiating quasigeostrophic vortices, *J. Phys. Oceanogr.*, 31, 2178–2185, doi:10.1175/1520-0485(2001)031<2178:DVORQV>2.0.CO;2.

Nycander, J., and M. B. Isichenko (1990), Motion of dipole vortices in a weakly inhomogeneous medium and related convective transport, *Phys. Fluids B*, 2(9), 2042–2047, doi:10.1063/1.859425.

Morrow, R., F. Birol, D. Griffin and J. Sudre (2004), Divergent pathways of cyclonic and anti-cyclonic ocean eddies, *Geophys. Res. Lett.*, 31, L24311, doi:10.1029/2004GL020974.

Simpson, J. J., and R. J. Lynn (1990), A mesoscale eddy dipole in the offshore California Current, *J. Geophys. Res. Oceans*, 95(C8), 13009–13022, doi:10.1029/JC095iC08p13009.

Southwick, O. R., E. R. Johnson, and N. R. Mcdonald (2015), A point vortex model for the formation of ocean eddies by flow separation, *Phys. Fluids*, 27, 016604, doi:10.1063/1.4906112.

Stern, M. E. (1975), Minimal properties of planetary eddies, *J. Mar. Res.*, 33(1), 1–13.

Strub, P. T., and C. James (2000), Altimeter-derived variability of surface velocities in the California Current System: 2. Seasonal circulation and eddy statistics, *Deep-Sea Res. II*, 47, 831–870, doi:10.1002/2015JC010769.

Supporting Information for

"Rapid water transport by long-lasting modon eddy pairs in the southern midlatitude oceans"

Chris W. Hughes[1], **Peter I. Miller**[2]

[1]University of Liverpool and National Oceanography Centre, Liverpool

[2]Plymouth Marine Laboratory

Contents

1. Figures S1 to S2

Additional Supporting Information (Files uploaded separately)

1. Captions for large Table S1
2. Captions for Movies S1 to S4

Introduction

Supplementary information consists of a table of modon vortex positions, and four movies showing the propagation of nine modons, and more detail for modon E. Below the descriptions of these separate files there are, included in this file, two figures. Supplementary Figure 1 (34 panels) shows detailed snapshots of sea surface temperature coinciding with modons B–E and J. Supplementary Figure 2 shows the structure of modon E with different spatial smoothing scales, and the matching analytical modon.

Table S1.

Table S1 contains estimated positions of vortex centers associated with each modon discussed in the paper (A–J). The file is a comma-separated-values (csv) file which can be read either as a text file or can be opened directly in Excel.

The table contains 5 columns. The first line is a header, and subsequent lines are all in identical format. The first column is a two-character identifier for the vortex, where the

---

Corresponding author: C. W. Hughes, `cwh@liv.ac.uk`

first character is the letter identifying the modon (A–J), and the second is a number 1–3 identifying the particular vortex (1 is the right-hand vortex, 2 is the left-hand vortex, and 3 is the second left-hand vortex in the case of modon H).

The second column is day number, with 1 representing 1993-01-01. The third column is longitude in decimal degrees east, in the range 0 to 360. The fourth column is latitude in decimal degrees north (the negative values therefore represent latitudes south of the equator). The final column is the date in the format year-month-day.

Movie S1.

Geostrophic current speed from satellite altimetry, from 5 January 1997 to 22 December 2012, in the region surrounding the southern part of Australia, with modons A–H highlighted by means of concentric black and white circles centered on each vortex of each modon, according to the positions listed in Table S1. In time, the ordering is modon A (east of Australia), modons F, G, H (west of Australia), modons B, C, D, E (east of Australia). The identification is purely subjective, and it may be possible to identify other modon events.

Movie S2.

Geostrophic current speed from satellite altimetry, for the period 16 April 2006 to 18 March 2008, in the region surrounding the southern part of Africa, with modon J highlighted by means of concentric black and white circles centered on each vortex of the modon, according to the positions listed in Table S1.

Movie S3.

Sea surface temperature (SST) anomaly associated with Modon E, from 21 May 2010 to 24 August 2011. The quantity plotted is temperature minus the median ocean temperature in the region plotted (a different median for each frame). The color scale saturates at $\pm 4\,°C$. The small black circles indicate the individual vortex centers as identified from geostrophic currents, and tabulated in Table S1. The SST product (described in the main text) represents a melding of high spatial resolution infra-red products which cannot see through cloud, and low spatial resolution microwave products which can see through cloud, explaining the varying sharpness in space and time.

Movie S4.

Sea surface temperature (SST) fronts during the eastward passage of Modon E, from 15 April 2010 to 28 February 2011. The fronts are identified as described in the main text from the variable-resolution SST data, which may explain why the fronts associated with the modon are clear at some times but not at others.

Supplementary Figures
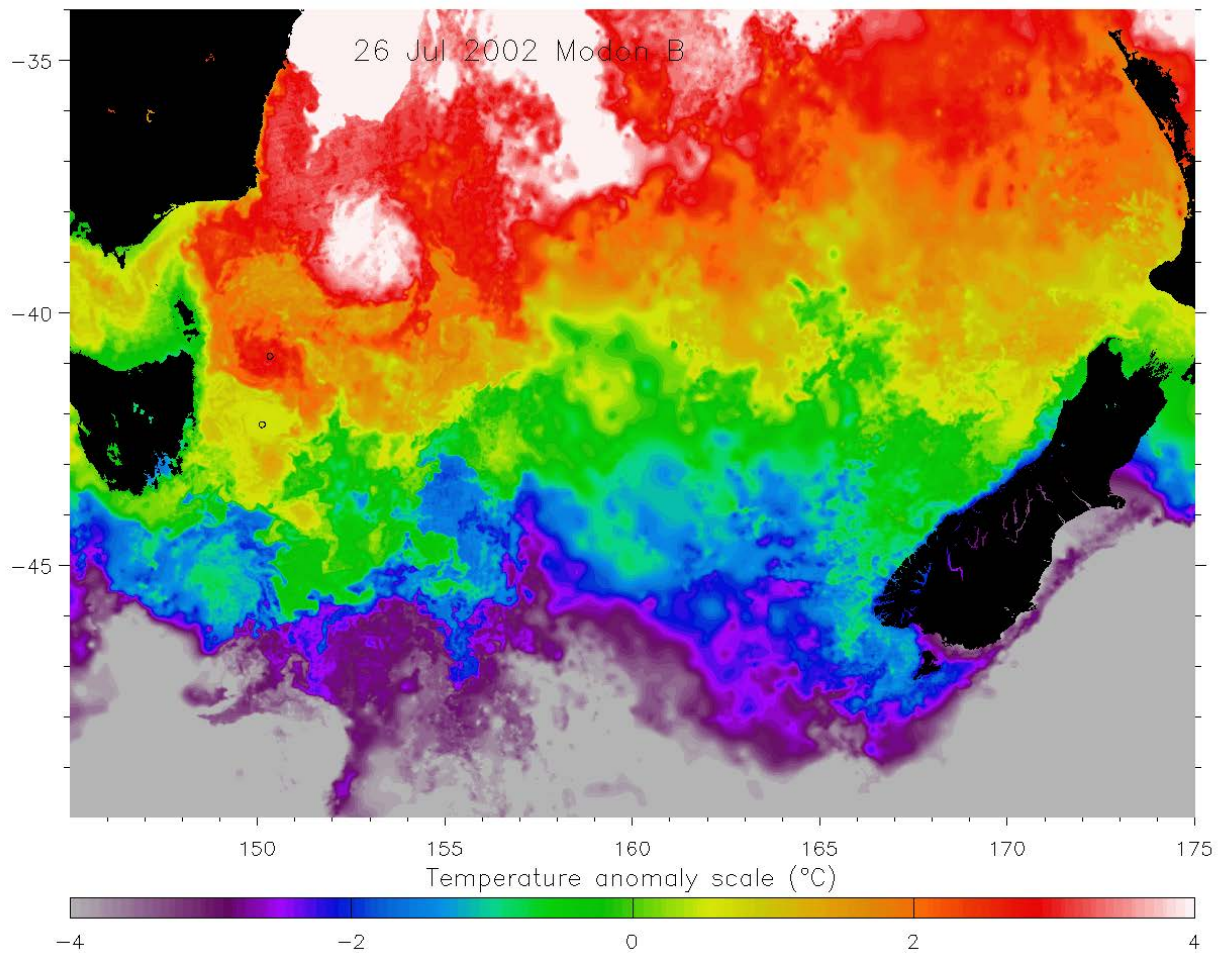
Figure S1. Snapshots of sea surface temperature coinciding with modon appearance. Black circles mark the two vortex positions as estimated from satellite altimetry. The date and relevant modon name are printed on each frame. Temperature is shown as the difference from the median value averaged over the shown ocean area.

Figure S1. Continued.
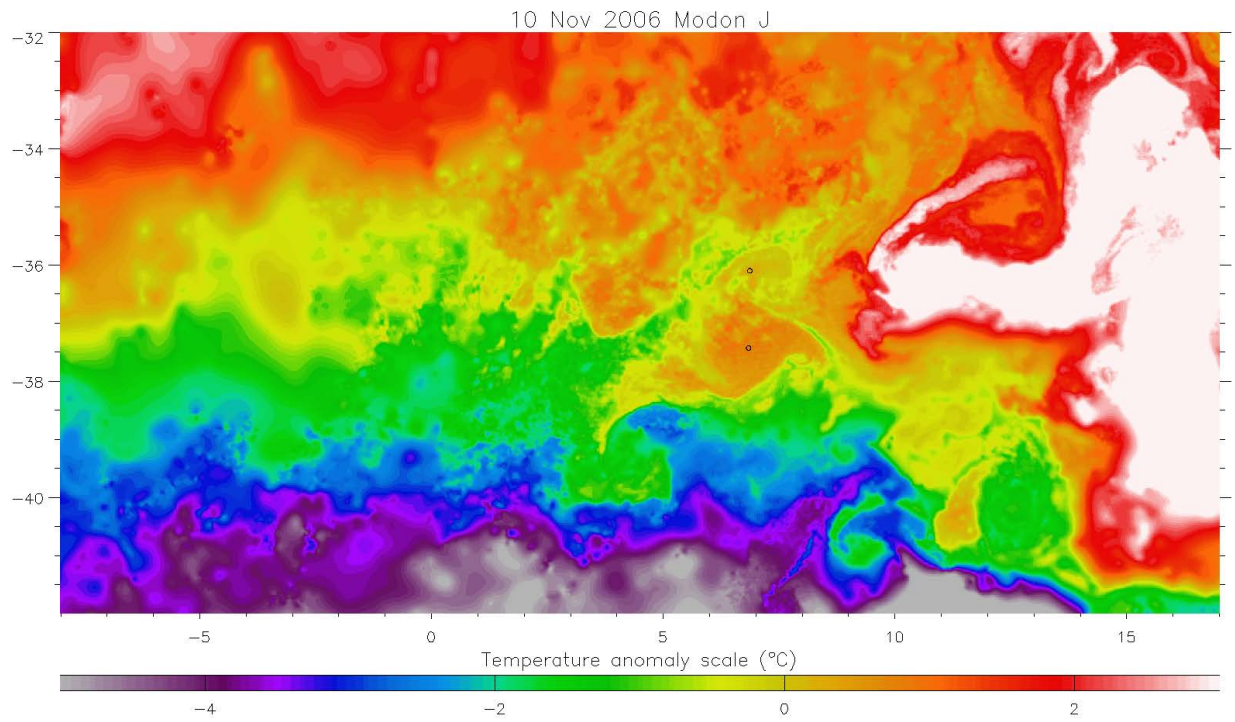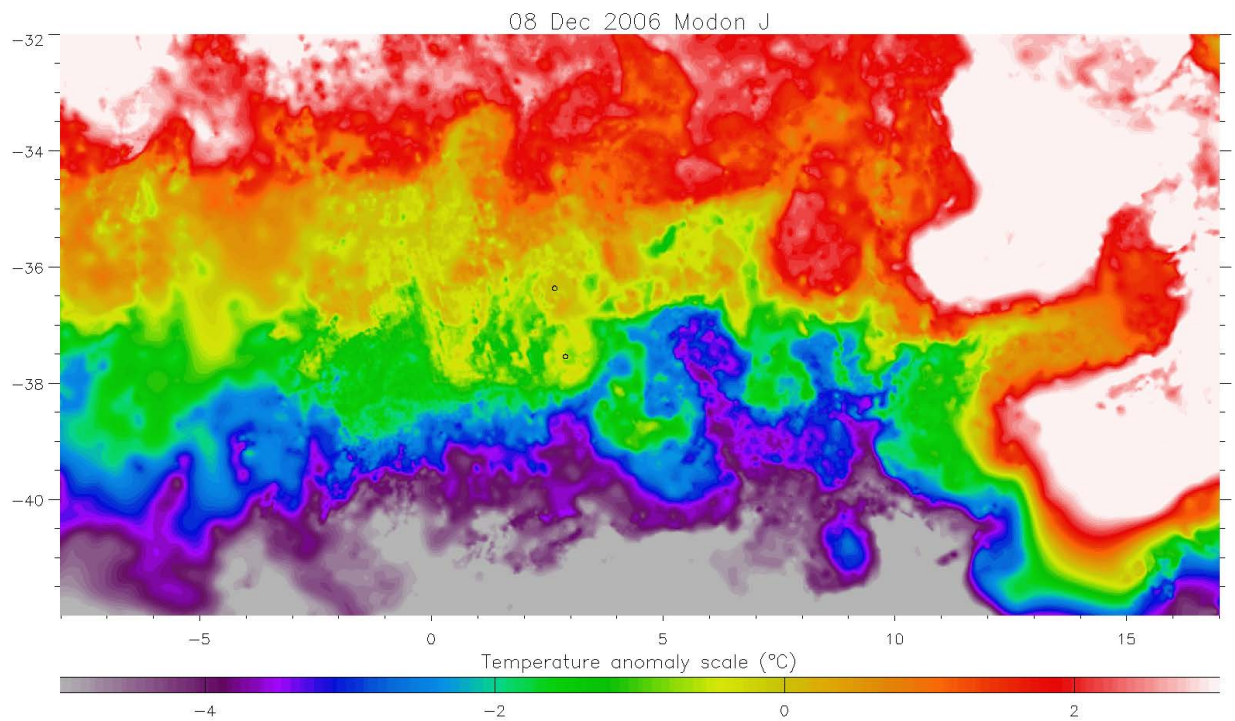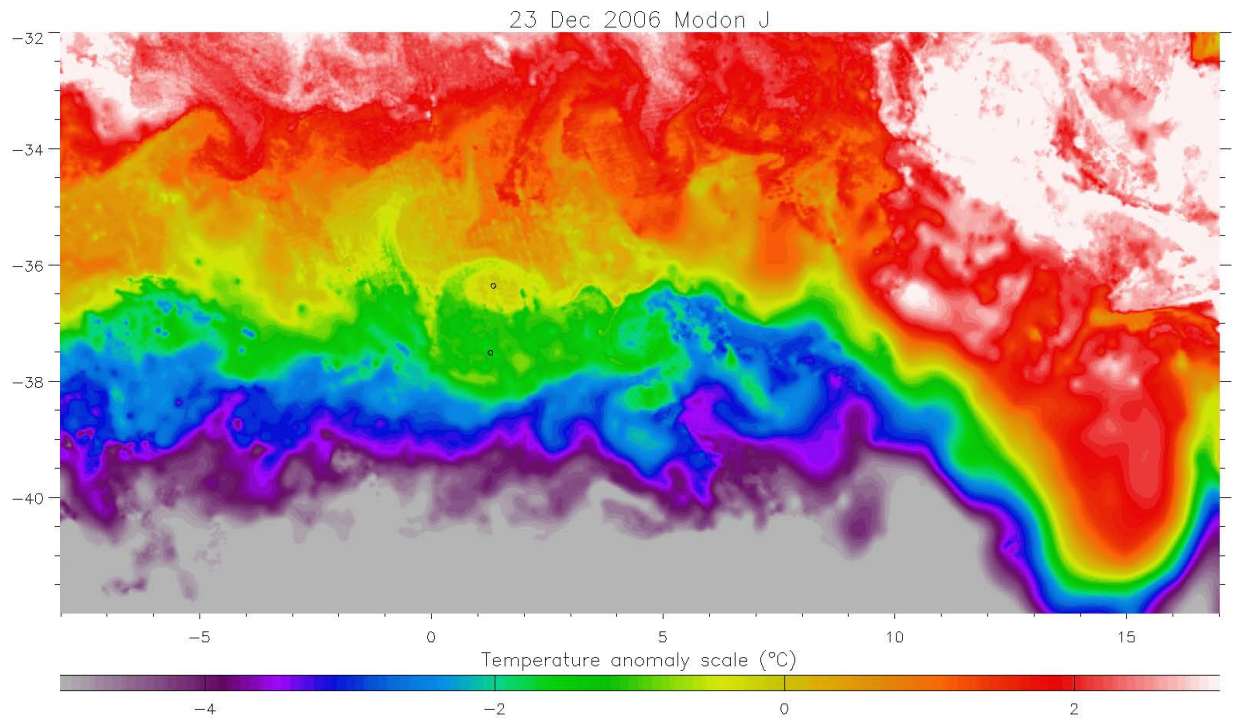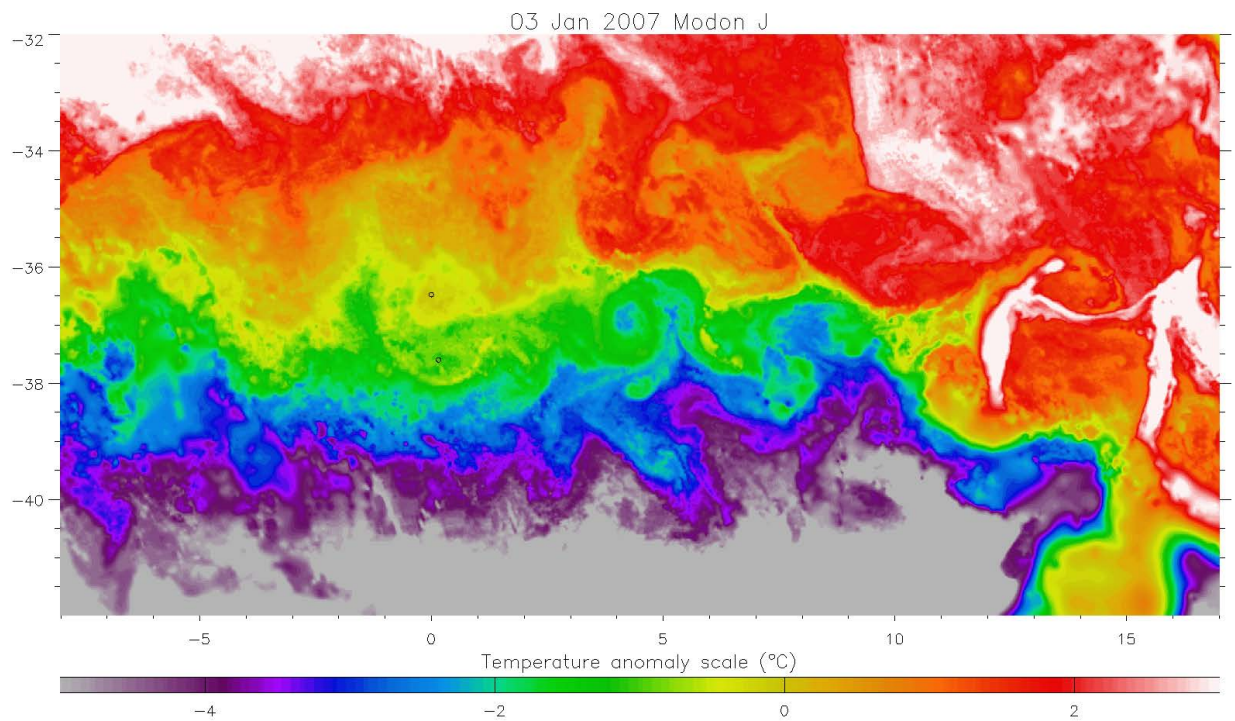
Figure S1. Continued.

Figure S1. Continued.

Figure S1. Continued.

06 Oct 2003 Modon C

Temperature anomaly scale (°C)

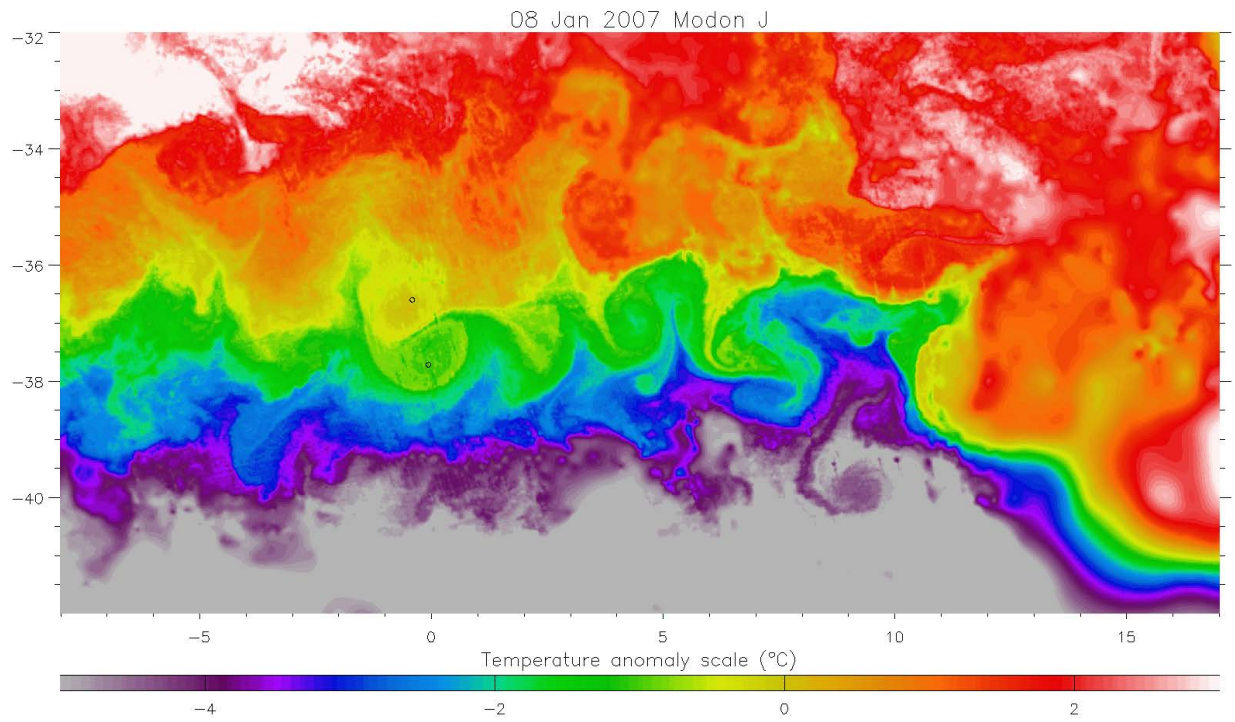**Figure S1.** Continued.

Figure S1. Continued.

Figure S1. Continued.

Figure S1. Continued.

Figure S1. Continued.

04 Mar 2006 Modon D

Temperature anomaly scale (℃)

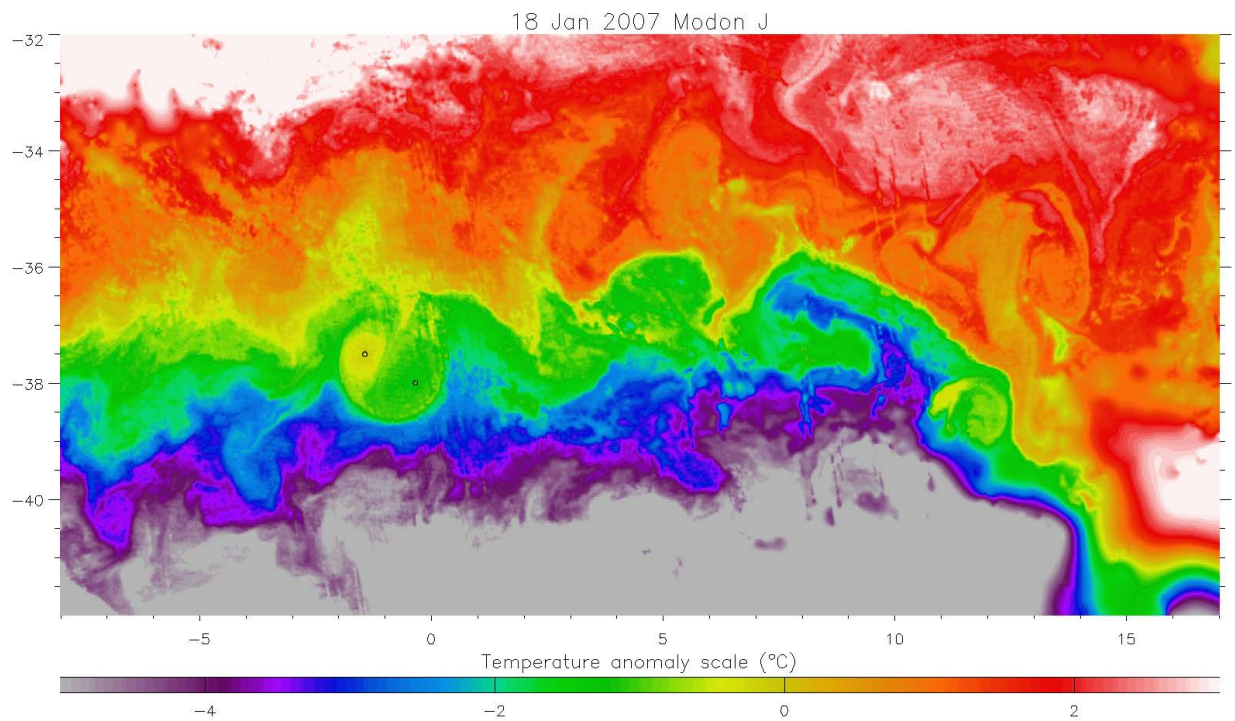**Figure S1.** Continued.

Figure S1.   Continued.

Figure S1. Continued.

Figure S1. Continued.

23 Sep 2006 Modon D

Temperature anomaly scale (°C)

Figure S1. Continued.

Figure S1.   Continued.
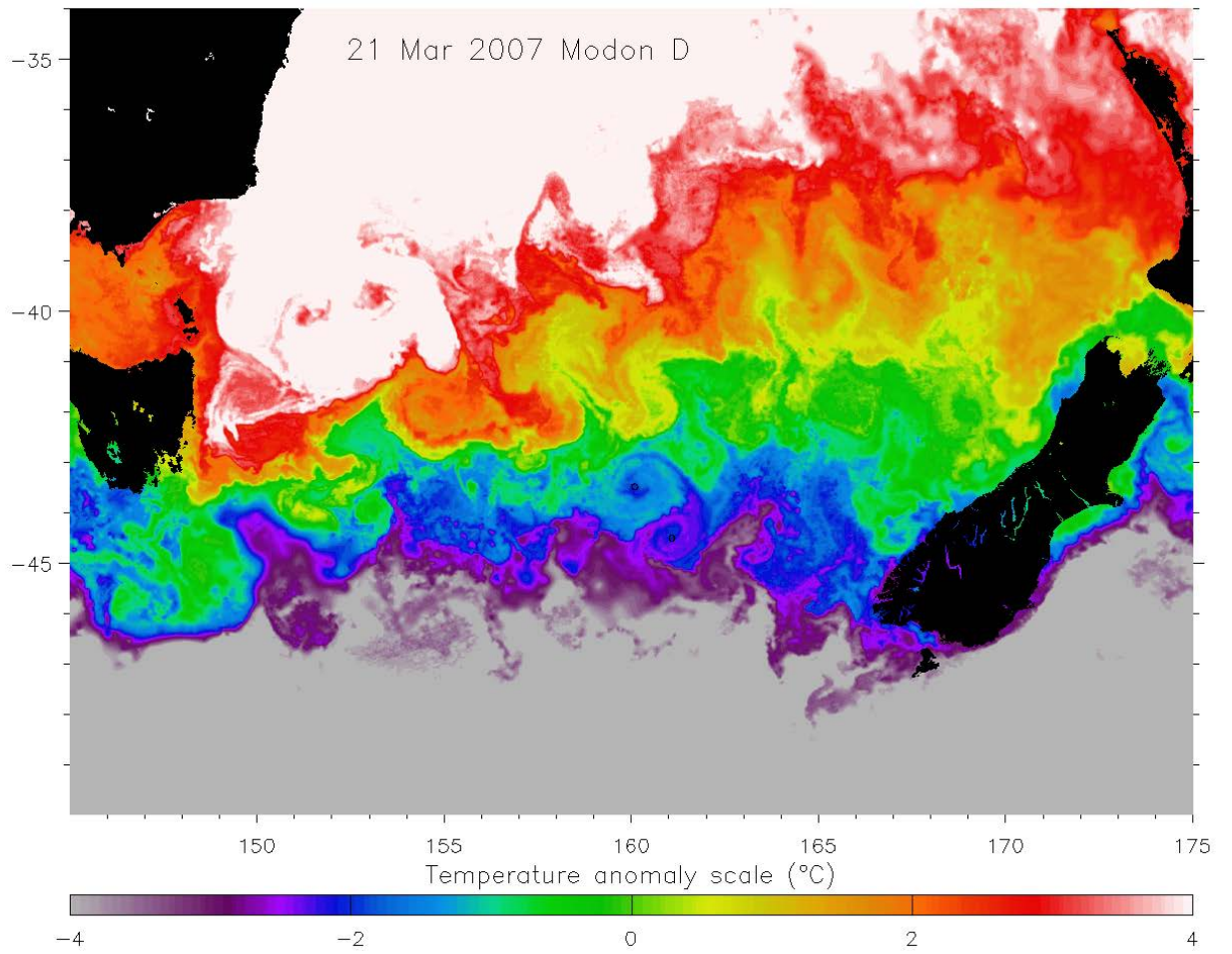
Figure S1.   Continued.
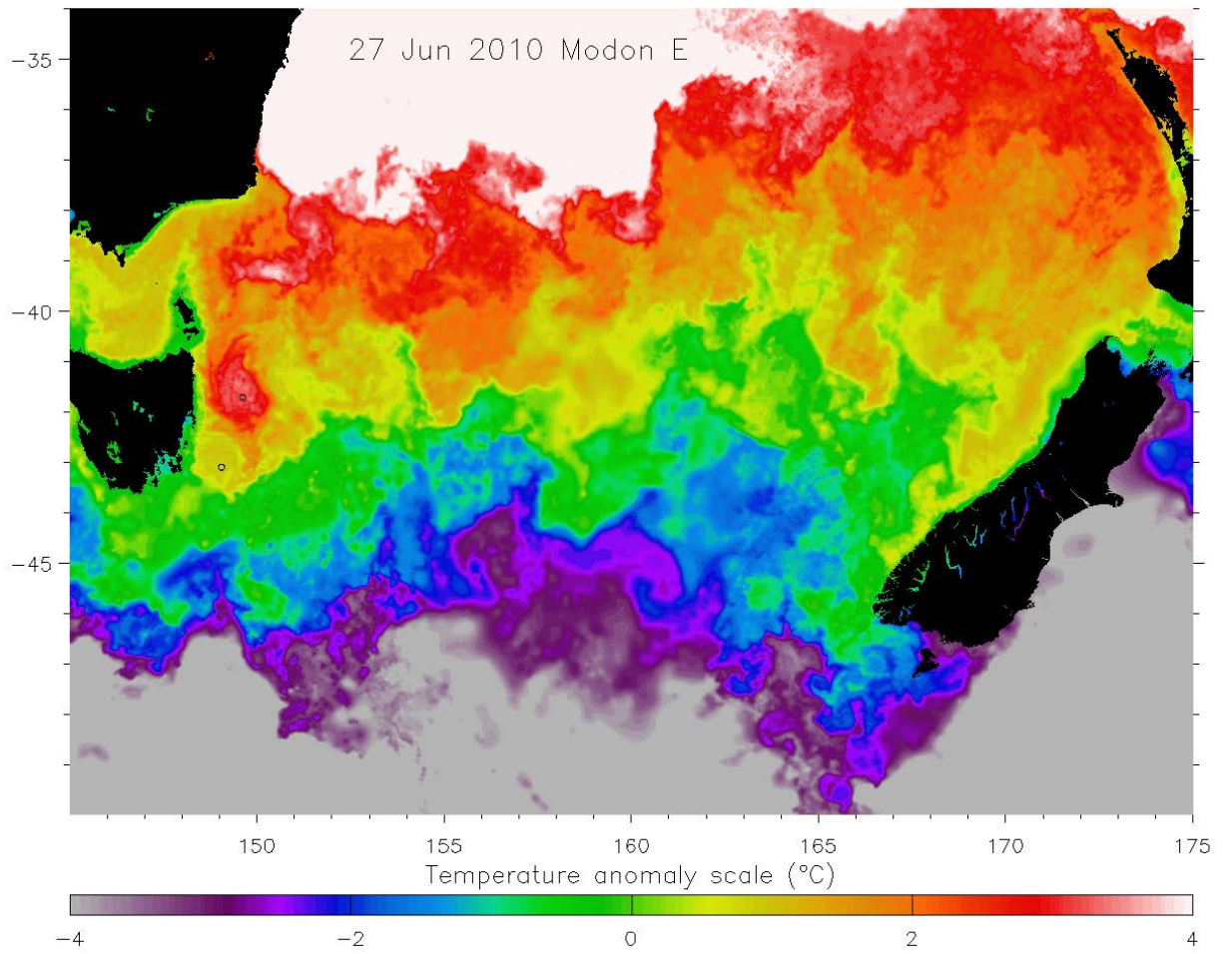
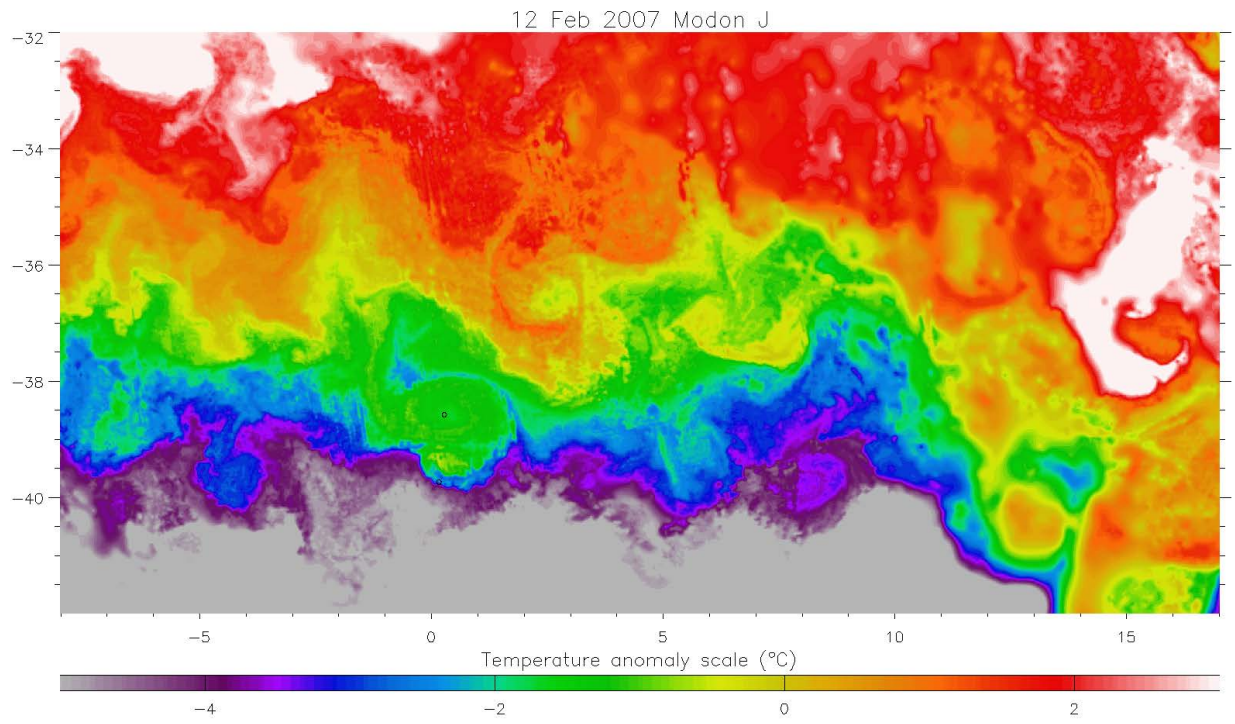**Figure S1.** Continued.
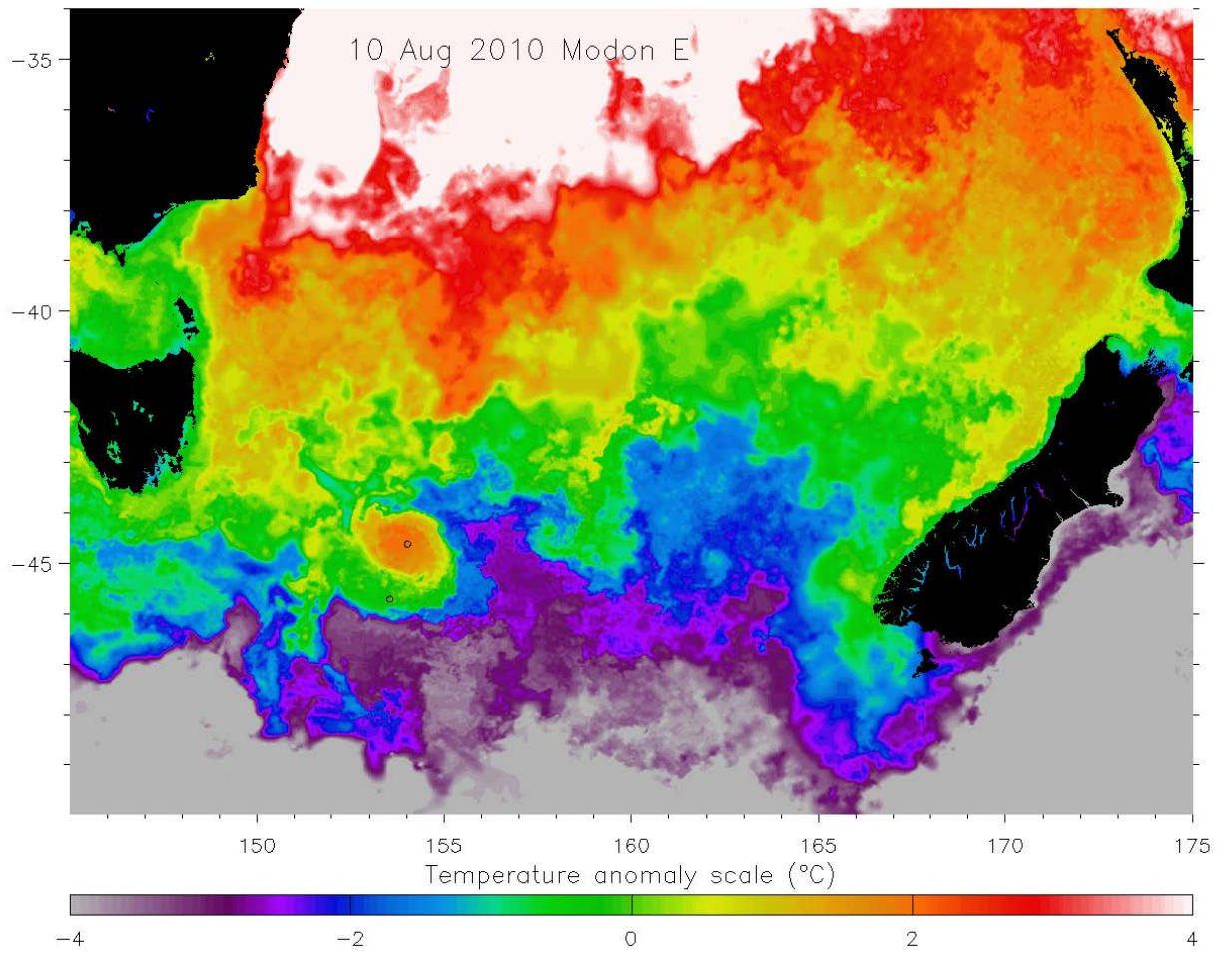
Figure S1. Continued.
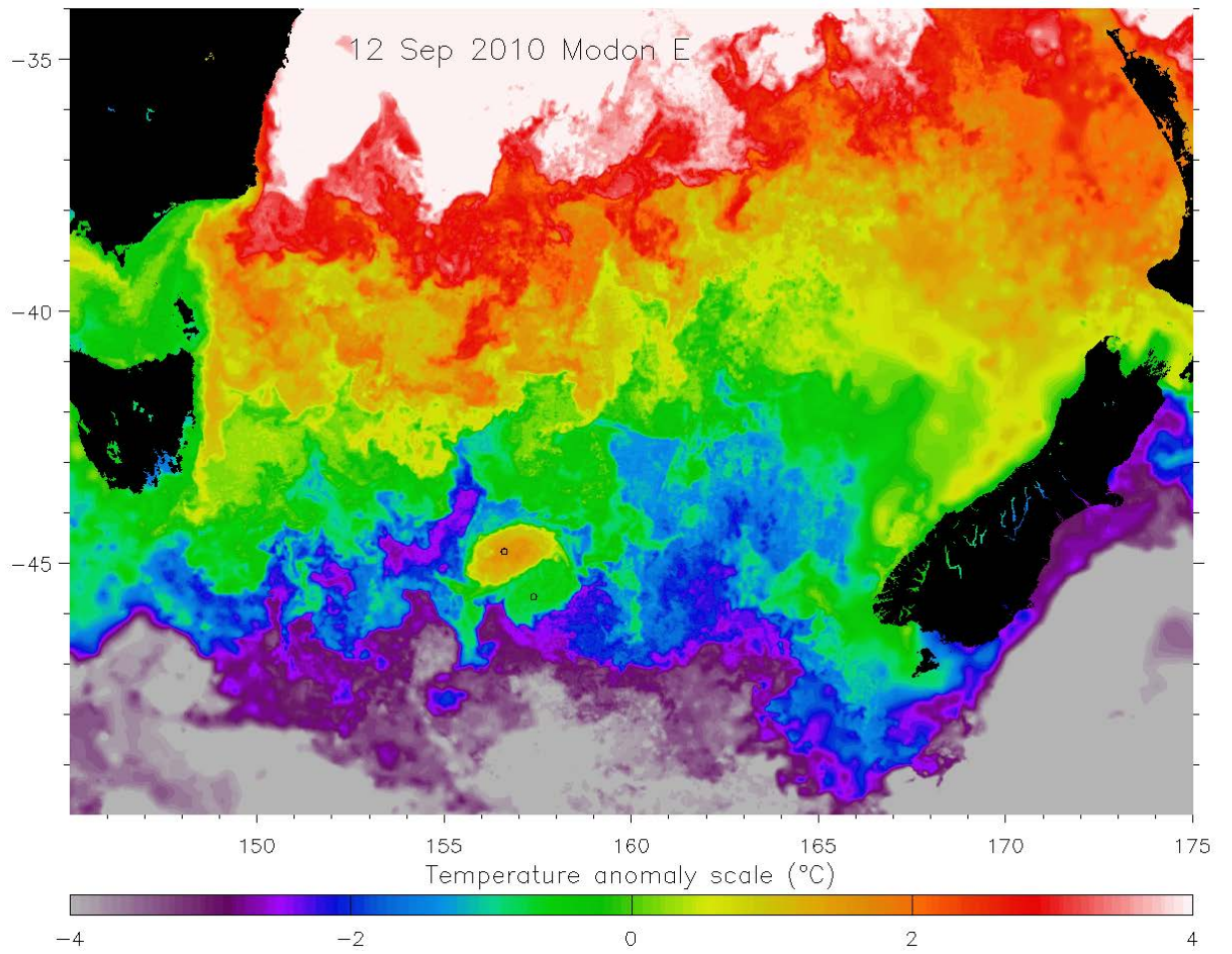
Figure S1. Continued.

Figure S1. Continued.

Figure S1. Continued.

Figure S1. Continued.

Figure S1. Continued.

Figure S1. Continued.

Figure S1. Continued.

Figure S1. Continued.

Figure S1. Continued.

Figure S1. Continued.

Figure S1. Continued.
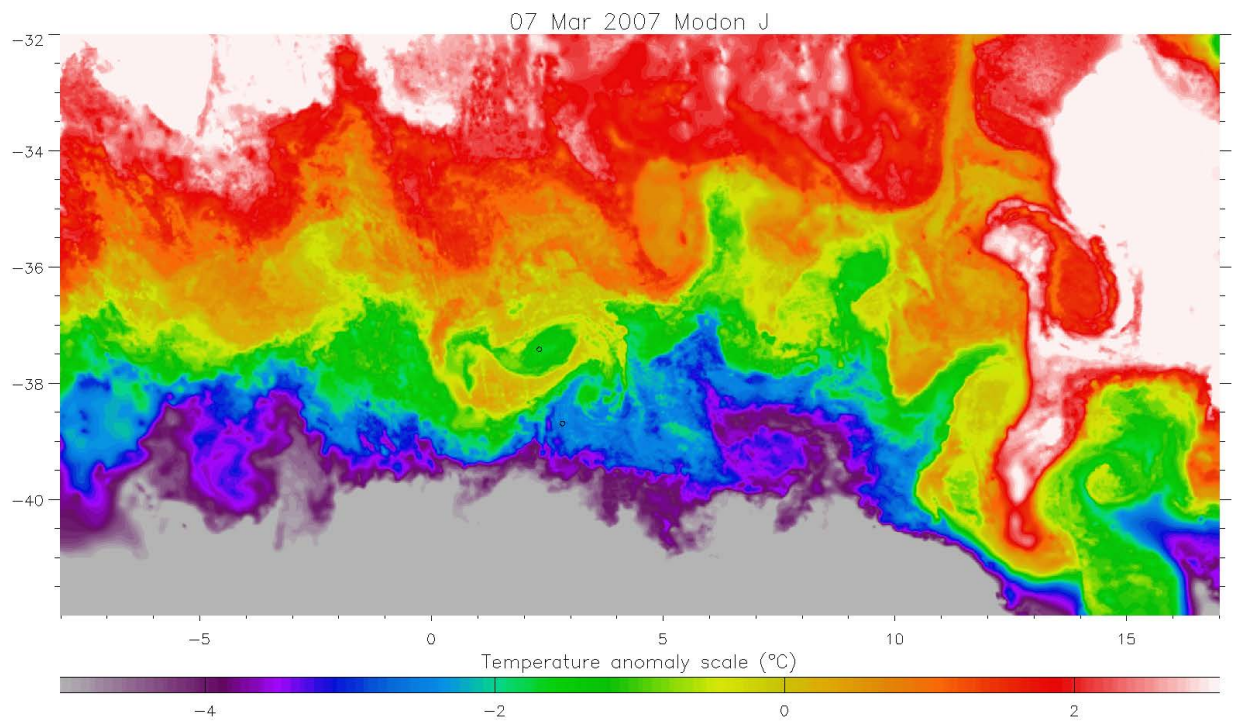

Figure S1. Continued.

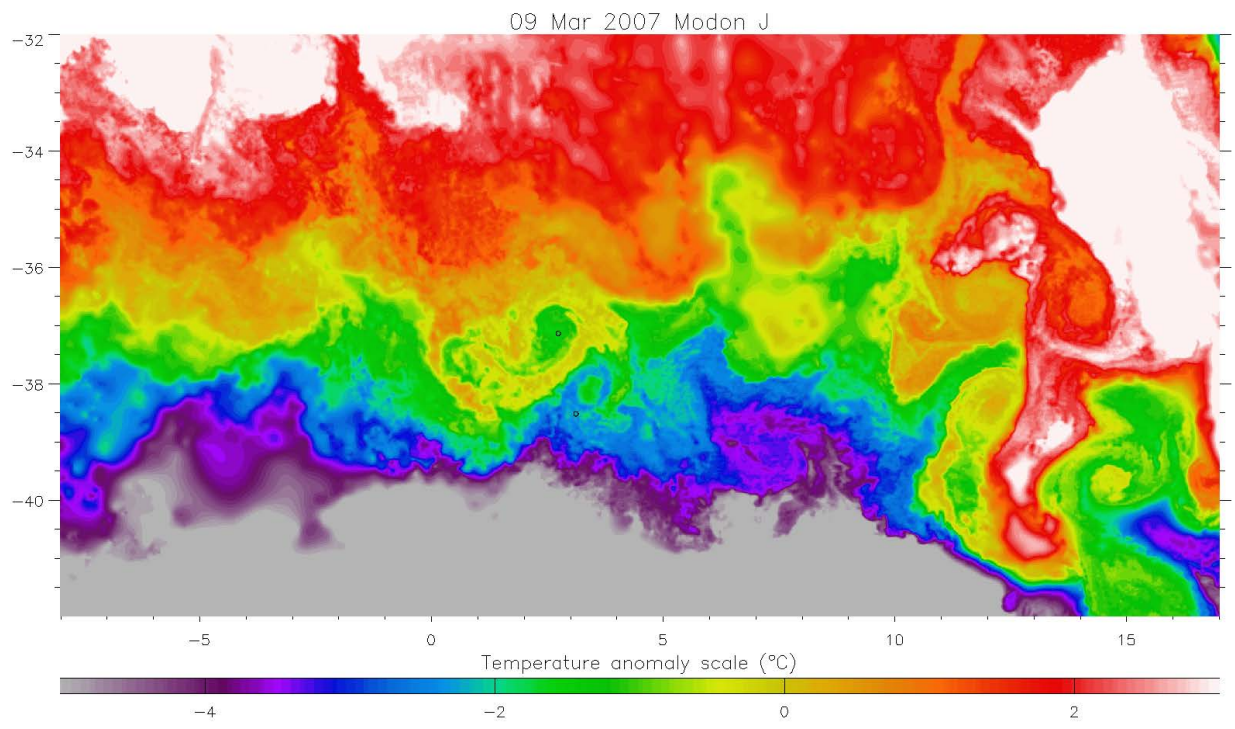**Figure S1.** Continued.

Figure S1. Continued.
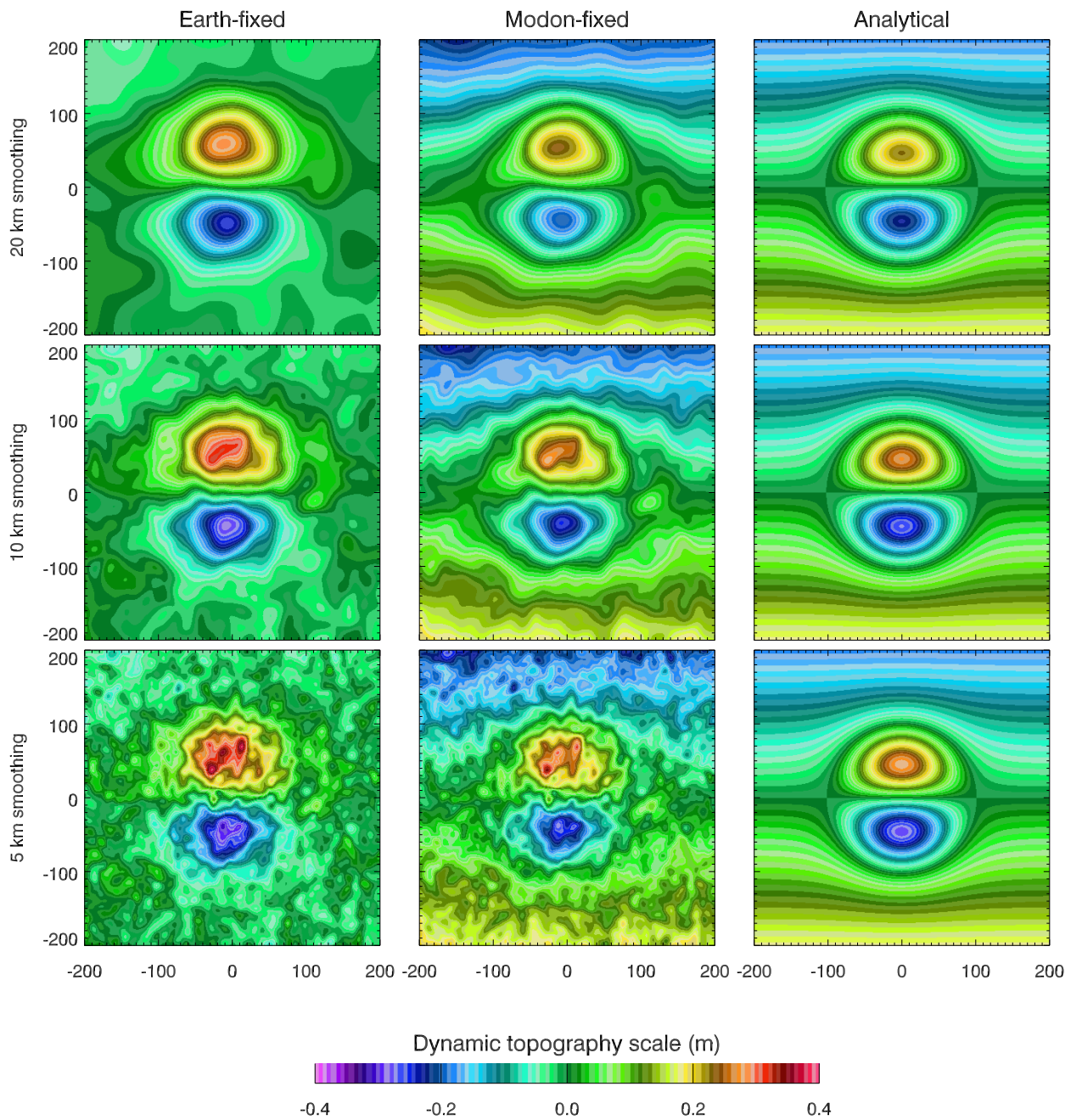
Figure S1. Continued.

Figure S2. Modon E mapped as described in the main text, but using different Gaussian smoothing scales. The scales are Gaussian radius at half maximum, and are 5 km (bottom), 10 km (middle) and 20 km (top). As in Figure 3, the modon is shown as measured (left) and corrected for an 8.8 cm s^{-1} eastward propagation speed (center). The right hand column shows the matching analytical modon with the same smoothing applied. The analytical modon was chosen by fitting to the 5 km-smoothed observations to minimise any scale change from the smoothing.